Improved Voltage Drop Compensation Method for Hybrid Fuel Cell Battery System

Tae-Ho Eom [1], Jin-Wook Kang [1], Jintae Kim [1], Min-Ho Shin [1], Jung-Hyo Lee [2] and Chung-Yuen Won [1],*

[1] Department of Electrical and Computer Engineering, Sungkyunkwan University, Suwon 16419, Korea; taehooo@skku.edu (T.-H.E.); kjw2171@naver.com (J.-W.K.); jintae.kim75@gmail.com (J.-T.K.); smh5480@nate.com (M.-H.S.)
[2] Department of Electrical Engineering, Kunsan National University, Kunsan 54150, Korea; jhlee82@kunsan.ac.kr
*   Correspondence: woncy@skku.edu; Tel.: +82-031-290-7164

check for updates

Abstract: In this paper, a voltage drop compensation method for hybrid hydrogen fuel cell battery system, with a hydrogen recirculation powering a forklift, is studied. During recirculating hydrogen fuel to recycle hydrogen that has not reacted enough at the system, impurities can be mixed with the hydrogen fuel. This leads to low hydrogen concentration and a drop in the output voltage of the fuel cell system. In excessive voltage drop, the fuel cell system can be shutdown. This paper proposes a voltage drop compensation method using an electrical control algorithm to prevent system shutdown by reducing voltage drop. Technically, voltage drop is typically caused by three kinds of factors: (1) The amount of pure hydrogen supply; (2) the temperature of fuel cell stacks; and (3) the current density to catalysts of the fuel cell. The proposed compensation method detects voltage drop caused by those factors, and generates compensation signals for a controller of a DC–DC converter connecting to the output of the fuel cell stack; thus, the voltage drop is reduced by decreasing output current. At the time, insufficient output current to a load is supplied from the batteries. In this paper, voltage drop caused by the abovementioned three factors is analyzed, and the operating principle of the proposed compensation method is specified. To verify this operation and the feasibility of the proposed method, experiments are conducted by applying it to a 10 kW hybrid fuel cell battery system for a forklift.

Keywords: fuel cell; hydrogen recirculation; voltage drop; compensation method; fuel cell forklift

1. Introduction

Throughout recent decades, renewable energies and hydrogen energy for electric vehicles have been studied as alternative power source for the conventional internal combustion engines, and to improve environmental pollution by reducing carbon dioxide emitted to the air as environmental regulation is gradually tightened [1–3].

To decrease the carbon dioxide emission, research on fuel cell, lithium battery, and super capacitor have been actively progressing [4–7]. Among them, the hydrogen fuel cell has been a focus of many studies, as it is considered one of the solutions. Basically, electrical energy can be generated in the hydrogen fuel cell by the reaction of hydrogen and oxygen through the membrane, in which hydrogen is supplied externally as compressed hydrogen and oxygen is utilized in the atmosphere after being purified. Among the different types, the proton exchange membrane fuel cell (PEMFC) is widely utilized in independent applications, such as a fuel cell vehicle, due to advantages of a low operating temperature of less than 100 °C, high power density, and fast start-up [8–13].

Meanwhile, other battery technologies for electric vehicles have also been researched as alternatives to the conventional internal combustion engine. However, these other batteries for electric vehicles have the disadvantages of long battery charging time and short mileage, unlike the hydrogen fuel cell system, which offers higher energy density, shorter charging time, and better mileage [14–16].

In the past, research has been done to improve the performance of the fuel cell, including work on the dead-end method and hydrogen oversupply method [17–20]. The dead-end method is when the fuel cell outputs a large current, and fuel loss occurs due to flooding phenomenon, leading to the deterioration of the fuel cell [21–23]. For this reason, various solutions using the water management of fuel cell have been studied [24–34]. Results show that the addition of a recirculation line and solenoid valve alone can increase fuel utilization rate, at low cost. Furthermore, the operation time increases compared to the dead-end method. The other method is the hydrogen oversupply method, efficiency of which is low due to high hydrogen fuel consumption. For this reason, hydrogen recirculation, with high hydrogen utilization, has been widely used recently. Hydrogen recirculation is highly fuel efficient, because it recycles discharged hydrogen that has not reacted during the reaction process of oxygen and hydrogen [35].

However, the recycled hydrogen could contain impurities that are created during the recirculation process, which results in unstable electrical output characteristics. In addition, the output side of the fuel cell is typically connected to a DC–DC converter. Therefore, the operation of the DC–DC converter, which works to supply constant output voltage could cause the fuel cell voltage to drop. In the worst case scenario, the fuel cell may shut down due to severe voltage drop. For that reason, a voltage drop compensation method is needed to prevent system shutdown.

In this paper, three factors that cause voltage drop during hydrogen recirculation are analyzed: (1) The voltage drop varying depending on the amount of hydrogen supply; (2) the temperature of the fuel cell stack; and (3) the current density of platinum catalyst.

When hydrogen recirculation occurs, the amount of pure hydrogen supplied to the fuel cell can differ due to impurities. This results in fuel cell output voltage drop. This voltage drop during initial operation can vary depending on the temperature of the fuel cell, and inherent resistance can vary during steady state operation, depending on the current density of the platinum catalyst.

In this paper, an electrical compensation method is proposed, in order to overcome voltage drop in hybrid fuel cell battery system, using a hydrogen recirculation system for a forklift. The proposed compensation method has a function detects the three causations for the voltage drop, and generates compensation signals to the DC–DC converter. As a command of the compensation signal, the proposed method even decreases output current of the DC–DC converter, compulsively, to prevent fuel cell voltage drop, and uses an additional battery supply in case of a lack of output current during the operation of DC–DC converter [36–41]. Accordingly, the proposed compensation method can result in fuel cell battery shutdown caused by low voltage during hydrogen recirculation [41].

To verify the feasibility and validity of the proposed voltage drop compensation method, it is applied to the buck-boost converter for a fuel cell used by a forklift. The problem of fuel cell shutdown due to voltage drop during hydrogen recirculation is solved by applying the proposed method.

This paper is organized as follows: In Section 2, the fuel cell system configuration for forklift, and the advantages of the hydrogen recirculation system, are explained. The voltage characteristics of the fuel cell for the three factors for the voltage drops are also analyzed. In Section 3, the reason why the output voltage of the fuel cell stack drops during hydrogen recirculation is analyzed, and the proposed voltage drop compensation method of the buck-boost converter is introduced. In Section 4, the three factors that cause voltage drops in fuel cells is analyzed by experiment, and the feasibility and validity of the proposed control method are confirmed through the fuel cell forklift experiment. Finally, Section 5 provides the conclusion.

2. Analysis of Voltage Drop Characteristics of the Fuel Cell System during Hydrogen Recirculation

The fuel cell forklift system consists of a hybrid fuel cell battery system and a forklift, as shown in Figure 1. The rated power of the fuel cell for the forklift used in this paper is 10 kW. Additionally, the fuel cell system includes a recirculation function. The hybrid fuel cell battery system consists of a fuel stack of 50 cells, a 35 bar hydrogen tank that is able to supply 70 liter per minute (LPM) to the fuel cell stack, a lithium polymer battery pack with 13 cells-200 Ah, the buck-boost converter, and the total control unit (TCU). Among secondary batteries, the lithium polymer battery using polymer electrolyte is widely used because of its high power density [42]. It also controls the input current of the buck-boost converter by means of the controller area network (CAN) communication.
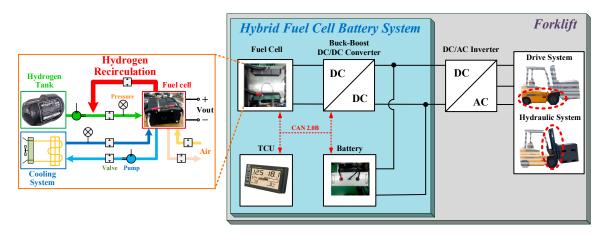

Figure 1. Configuration diagram of hybrid fuel cell battery for a forklift, including hydrogen recirculation. TCU, total control unit.

The forklift consists of an inverter, drive motor, and hydraulic motor. The inverter is designed with a power of 50 kW, which is used to simultaneously perform a 5 ton lift and drive the forklift.

In addition, the fuel cell used PEMFC, including hydrogen recirculation. In the system, compressed hydrogen from a hydrogen tank is supplied to the fuel cell stack. The supplied hydrogen reacts with oxygen in the atmosphere to generate electric energy. During the reactions between the two gases, some conditions can cause voltage drop due to several reasons. In a worst case scenario, the voltage drop at the PEMFC system can cause system shutdown. There are three main causal factors for this lack of hydrogen supply, temperature at the fuel cell stack, and the current density of the platinum catalyst.

Figure 2 shows voltage drop characteristics depending on current density loaded on the fuel cell system. In ideal state, an initial open circuit voltage (OCV) of a fuel cell unit is 1.2 V. The output voltage gradually decreases from the OCV as the load current increases. However, voltage drop can be drastically accelerated at area A because the electrochemical reaction is abruptly reduced as the hydrogen fuel is consumed. In addition, voltage drop of area A can be increased due to impurities during the hydrogen recirculation.

Meanwhile, a detailed explanation of the curve is given in Reference [35].

The output voltage of the fuel cell, v_{out}, can be described by subtracting the voltage drop, Δv_{drop}, from the OCV, V_{OCV}, in Equation (1). In addition, the voltage drop is determined by the three factors mentioned, above which can be expressed as Equation (2).

$$v_{out} = V_{OCV} - \Delta v_{drop}, \tag{1}$$

$$\Delta v_{drop} = \Delta v_{hydro} + \Delta v_{temp} + \Delta v_{den}, \tag{2}$$

where, Δv_{hydro} is voltage drop depending on amount of hydrogen supply, Δv_{temp} is voltage drop depending on temperature of a fuel cell stack, and Δv_{den} is voltage drop depending on the current density of platinum catalyst.
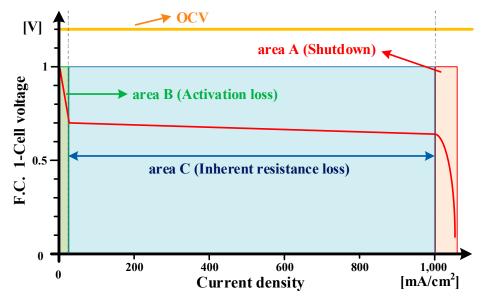

Figure 2. Voltage characteristic curve of fuel cell.

2.1. Voltage Drop Characteristics Depending on Hydrogen Supply

When the hydrogen recirculation is applied to the stacks, hydrogen usage can be reduced by recirculating the not-reacted hydrogen. The hydrogen recirculation is very easy to apply to conventional hydrogen fuel cell system by simply installing a hydrogen recirculation line and solenoid valve.

However, if the hydrogen containing impurities at the recirculation is supplied to the fuel cell stacks, their output voltage can be significantly decreased, as can be seen in Figure 3. The y-axis of Figure 3 is the fuel cell stack consisting of 50 cells voltage.
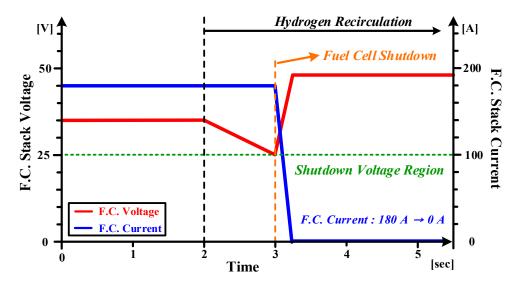

Figure 3. Fuel cell stack waveforms for conventional control method during hydrogen recirculation.

At the fuel cell unit, if the cell voltage is reduced to 0.5 V or less, the fuel cell stacks can be broken because high pressure applies to the separation membrane.

In order to generate high quality electricity, hydrogen fuel and oxygen have to be continuously supplied in the fuel cell. Equation (3) shows relationship between a voltage drop and hydrogen supply.

$$\Delta v_{hydro} = \frac{RT}{2F} \ln\left(\frac{P_{H_2}}{P_{H_2O}}\right) + \frac{RT}{2F} \ln\left(P_{O_2}\right)^{\frac{1}{2}}, \tag{3}$$

where,

$$\begin{cases} R = universal\ gas\ constant\ (8.314\ \mathrm{J/mol\cdot K}) \\ T = kelvevin\ temperature\ (\mathrm{K}) \\ F = farada's\ constant\ (96,485\ \mathrm{C/mol}) \\ P_{H_2} = hydrugen\ partial\ pressure\ (\mathrm{LPM}) \\ P_{O_2} = oxygen\ partial\ pressure\ (\mathrm{LPM}) \\ P_{H_2O} = water\ partial\ pressure\ (\mathrm{LPM}) \end{cases} .$$

Figure 4 shows a graph of voltage drop depending on hydrogen supply, plotted based on Equation (3). For example, when hydrogen supply is 60 LPM continuously, then the fuel cell can support maximally a 200 A load condition. Meanwhile, if hydrogen supply is reduced to 40 LPM due to impurities in the hydrogen recirculation, it can be estimated that the fuel cell can be damaged at a 110 A load current. Namely, voltage drop can be easily anticipated by measuring hydrogen supply and Equation (3).
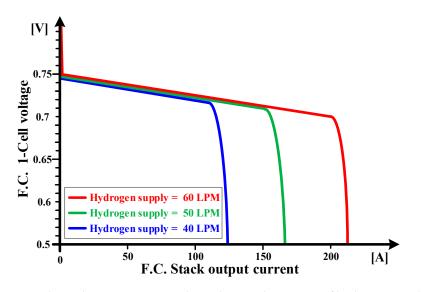

Figure 4. Voltage characteristic curve depending on the amount of hydrogen supply.

2.2. Voltage Drop Characteristics Depending on Temperature of the Fuel Cell Stack

Besides the hydrogen supply, a voltage drop depends on temperature of the fuel cell stack. The area B of Figure 2 is the voltage drop caused by the activation polarization, and it varies depending on temperature of the fuel cell stack.

Figure 5 shows the output voltage Δv_{out} of the fuel cell decrease as the temperature increases. Since the fuel cell used in vehicle requires a fast starting time, the operating temperature is controlled to 60 °C–70 °C.
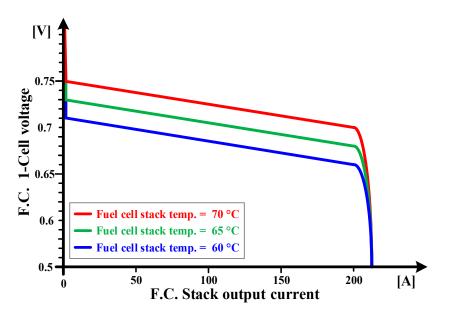
Figure 5. Voltage characteristic curve depending on the temperature of fuel cell stack.

The voltage drop Δv_{temp} is predicted, as shown in Equation (4) from the Butler Volmer equation. Δv_{temp} appears to increase linearly as the temperature increase. However, when the temperature is increased, the exchange current density, i_o, is heavily decreased based on Equation (5). Therefore, Δv_{temp} is heavily reduced.

$$\Delta v_{temp} = \frac{RT}{\alpha F} \ln(i/i_o), \tag{4}$$

where,

$$\begin{cases} \alpha = transfer\ coefficient\ (0 \sim 1) \\ i = current\ density\ (\text{A}/\text{cm}^2) \\ i_o = exchange\ current\ density\ (\text{A}/\text{cm}^2) \end{cases},$$

$$i_o = nFK_{o,f}C_{Ox}exp\left[\frac{-\alpha_{Rd}FE_r}{RT}\right] \tag{5}$$

where,

$$\begin{cases} n = number\ of\ moles\ of\ electrons\ (6.022 \times 10^{23}) \\ K_{o,f} = forward\ reaction\ rate \\ \alpha_{Rd} = charge\ transfer\ coefficient\ of\ reduction\ reaction \\ C_{Ox} = surface\ soncentration\ of\ oxidation\ reaction\ (\text{mol}/\text{cm}^2) \\ E_r = standard\ reversible\ cell\ potential \end{cases},$$

2.3. Voltage Drop Characteristics Depending on Current Density of Platinum Catalyst

Platinum is mainly used as a catalyst for promoting the activation reaction of the fuel cell. Platinum catalyst is very efficient for the oxidation of hydrogen, but the oxygen reduction reaction (ORR) is slow. Because of this characteristic, the voltage drop is dependent on the current density of platinum catalyst. The current density of platinum catalyst represents the energy activity per unit area of the catalyst layer [43–45]. Area C of Figure 2 is the voltage drop depending on the current density of the platinum catalyst and the inherent resistance. Figure 6 shows the output voltage Δv_{out} of the fuel cell decrease as the catalyst current density increases. At high current density, the voltage drop effect large because the diffusion of reactants is slow.
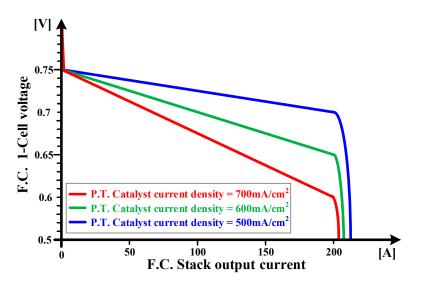
Figure 6. Voltage characteristic curve depending on the current density of platinum catalyst.

All conductors have inherent resistance, R_{ir}, that causes the voltage drop, Δv_{den}, in the flow of charges. When R_{ir} and cross section of the catalyst A_{cell} are constant, the voltage drop varies with the current density of platinum catalyst, i_{pc}. Δv_{den} is calculated, as shown in Equation (6) from the Ohm's law.

$$\Delta v_{den} = A_{cell} i_{pc} R_{ir}, \tag{6}$$

where,

$$\begin{cases} A_{cell} = active\ cell\ area\ (\mathrm{cm^2}) \\ i_{pc} = current\ density\ (\mathrm{A/cm^2}) \\ R_{ir} = inherent\ resistance\ (\Omega) \end{cases},$$

As explained previously, a voltage drop can be predicted by calculating the above three factors. Thus, the proposed compensation method in Section 3 prevents shutdown of the fuel cell system due to voltage drop.

3. The Proposed Voltage Drop Compensation Method of Buck-Boost Converter Considering Voltage Drop during Hydrogen Recirculation

In Section 2, the three factors that cause voltage drop of the hydrogen fuel cell system were analyzed. The first is the voltage drop depending on the amount of hydrogen supply. The voltage drop varies as the amount of hydrogen supply decreases in the operation of the fuel cell. This situation usually happens due to influx of impurities during hydrogen recirculation. Even the impurities cause that the fuel cell system may shutdown due to excessive voltage drop, as shown in Figure 3. The amount of hydrogen supplied to the fuel cell stack is sensed through the sensing device as in Reference [33]. In addition, other factors affecting voltage drops are the temperature of fuel cell stack and current density of the platinum catalyst.

Figure 7 shows the control block diagram of the buck-boost converter that compensates for voltage drop due to these three factors. As shown in the control block diagram, the proposed control algorithm includes three different compensation values, corresponding to each of the voltage drop factors.

Firstly, Δv_{hydro} represents the compensation value of the voltage drop depending on the amount of hydrogen supply. The compensation value of the voltage drop depending on the measured hydrogen, H_{stack}, supplied to the fuel cell, including recirculated hydrogen can be calculated using Equation (3). In addition, the Δv_{hydro} value increases as more impurities. Δv_{hydro} is used to calculates the Δv_{drop} as Equation (2). The voltage compensation is performed by decreasing reference current I_{in}^*, which is the reference current of the current controller according to the ratio of the calculated voltage drop.
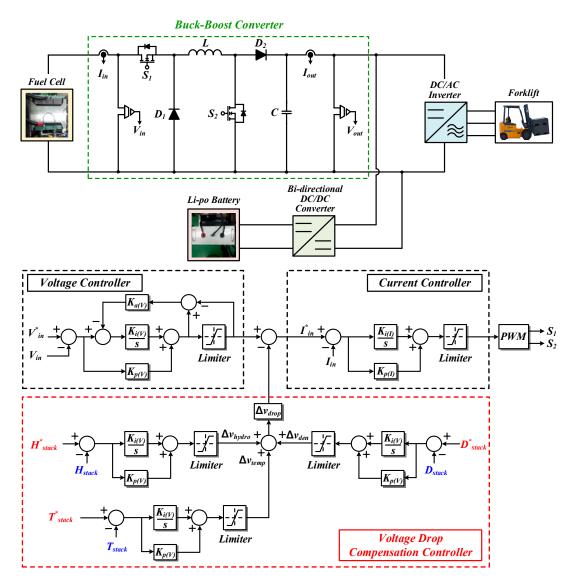
Figure 7. Control block diagram of the proposed voltage drop compensation method.

Secondly, Δv_{temp} is the compensation value of the voltage drop depending on the temperature of the fuel cell stack. Δv_{temp} varies frequently as the fuel cell operates. Therefore, the temperature of the fuel cell stack T_{stack}, is continuously sensed to estimate Δv_{temp} using Equation (4).

Thirdly, Δv_{den} is the compensation value of the voltage drop depending on the current density of platinum catalyst D_{stack}. The higher D_{stack} is, the faster the electrochemical reaction rate due to the increased exchange current density. However, when D_{stack} is high, the voltage drop due to the inherent resistance of the fuel cell increases, as shown in Equation (6). Therefore, in this paper, the current density of platinum catalyst is set to 700 mA/cm^2, which is adequate considering the capacity of the fuel cell, and the compensation value Δv_{den} is calculated through Equation (6).

Using those three calculated control values, Δv_{hydro}, Δv_{temp}, Δv_{den}, voltage drop, Δv_{out}, is estimated by Equation (2), and the voltage drop compensation is performed by feed-forwarding the estimated voltage drop into the input of the current controller, as shown in Figure 7.

Figure 8a shows the simulation waveforms that prove the proposed voltage drop compensation method prevents shutdown of the fuel cell during hydrogen recirculation by adjusting the output current of the fuel cell from 180 A to 170 A. As the current supplied from the fuel cell decreases, the output current from the lithium polymer battery parallel-connected to the fuel cell increases to meet the load requirement.
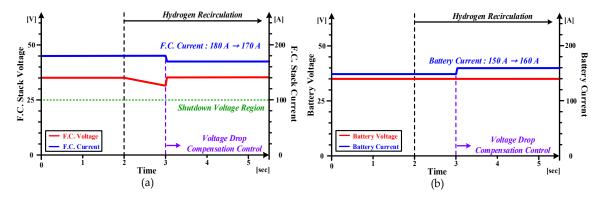
Figure 8. Voltage and current waveforms with proposed voltage drop compensation method during hydrogen recirculation for (**a**) fuel cell stack and (**b**) lithium polymer battery.

Figure 8b shows the simulation waveforms when the output current of the battery increases after compensating for the voltage drop. The battery current supplied to the load has increased from 150 A to 160 A.

Figure 9 shows the supplied power variation to the load when the proposed compensation method is operating. As shown in Figure 9, the battery supplies as much extra power as the decreased fuel cell power during the voltage drop compensation due to hydrogen recirculation, maintaining the power supplied to the load. Thus, using the proposed compensation control, constant power can be supplied to the load.
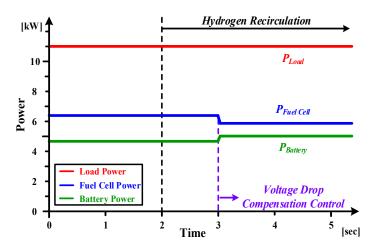

Figure 9. Output power waveforms of load, fuel cell and battery.

4. Experiment Results

4.1. The Experiment Hardware Configuration

The hardware configuration of the buck-boost converter for applying the proposed voltage drop compensation method is shown in Figure 10. The size reduction of the fuel cell system is required because a hybrid fuel cell battery system is placed in limited area of electric forklift. In order to reduce the size, module type device is used that combined MOSFET and the diode. In addition, the pin-type heat sink is used to reduce the size of the cooling system, and TMS320F28335 is used as a microprocessor for the TCU. The electrical specification of the buck-boost converter is shown in Table 1. The rated power is 10 kW, and it operates at 25 kHz of high switching frequency to minimize output ripple.
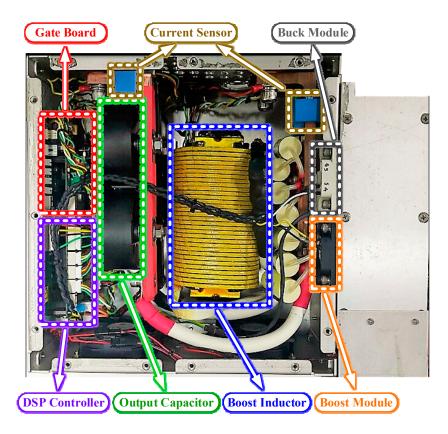
Figure 10. Busk-boost converter hardware configuration.

Table 1. The electrical specification of the buck-boost converter.

Parameters	Values	Units
Rated power	10	[kW]
Input voltage	30~50	[V_{DC}]
Input current	200	[A_{DC}]
Output voltage	42~54	[V_{DC}]
Output current	200	[A_{DC}]
Output ripple	±2	[%]
Switching frequency	25	[kHz]
Boost inductor	200	[μH]
Output capacitor	50	[μF]

4.2. The Voltage Drop Characteristics of the Three Factors

The characteristics of an estimated voltage drop, that could take place in three circumstances analyzed in Section 2, are verified through experiments. First, the voltage drop variation depending on the amount of hydrogen supplied to the fuel cell stack is verified. Table 2 shows the experimental conditions of the output characteristics depending on the amount of hydrogen supplied to the fuel cell stack.

Table 2. Characteristics experimental conditions of fuel cell.

Parameters	Values	Units
Hydrogen supply	50–70	[LPM]
Stack temperature	60	[°C]
Current density	700	[mA/cm^2]

As per the experiment results shown in Figure 11a–c, it can be confirmed that the operating range of the fuel cell increases as the amount of hydrogen supplied increases. In addition, Figure 11d shows the voltage drop graph depending on the amount of hydrogen supply through the experiment result. If the amount of hydrogen supply is low, shutdown may occur. In this paper, when performing drive experiment of forklift, the amount of hydrogen supply is 70 LPM.
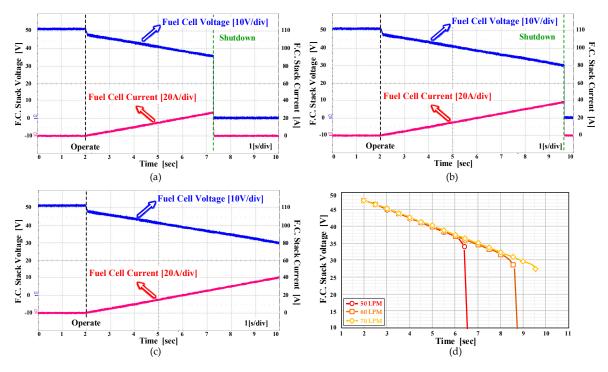

Figure 11. Fuel cell waveforms for supplied hydrogen of (**a**) 50 LPM, (**b**) 60 LPM, (**c**) 70 LPM, and (**d**) voltage drop curve depending on the amount of hydrogen supply.

Second, the voltage drop depending on the temperature variation of the fuel cell is verified, which is related to the magnitude of the output voltage of the fuel cell. Table 3 shows the experimental conditions of the output characteristics depending on the temperature of the fuel cell stack.
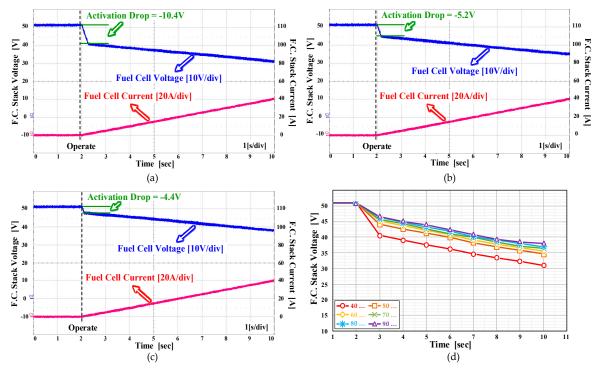
Table 3. Characteristic experimental conditions of fuel cell.

Parameters	Values	Units
Hydrogen supply	70	[LPM]
Stack temperature	40–90	[°C]
Current density	700	[mA/cm^2]

As per the experiment results, shown in Figure 12a–c, it can be confirmed that the voltage drop decrease as the temperature of fuel cell stack increases. In addition, Figure 12d shows the voltage drop graph depending on the temperature of the fuel cell stack. In accordance with experiment results, it is beneficial to operate the system at high temperature, but the temperature should be controlled to 70 °C or less because of the forklift application requirement.

The last factor is the voltage drop depending on the current density of the platinum catalyst. It is mostly caused by the IR drop due to the inherent resistance of the fuel cell. Table 4 shows experimental conditions of the fuel cell stack with the current density of platinum catalyst variation.

As per the experiment results shown in Figure 13a–c, it can be confirmed that the voltage drop increases as the current density of the platinum catalyst increases. In addition, Figure 13d shows the voltage drop graph depending on the current density of the platinum catalyst. In this paper,

when performing the forklift drive and lift experiment, the current density of the platinum catalyst is 700 mA/cm^2.

Figure 12. Fuel cell waveforms for stack temperature of the (**a**) 40 °C, (**b**) 70 °C, (**c**) 90 °C, and (**d**) voltage drop curve depending on the temperature of fuel cell stack.
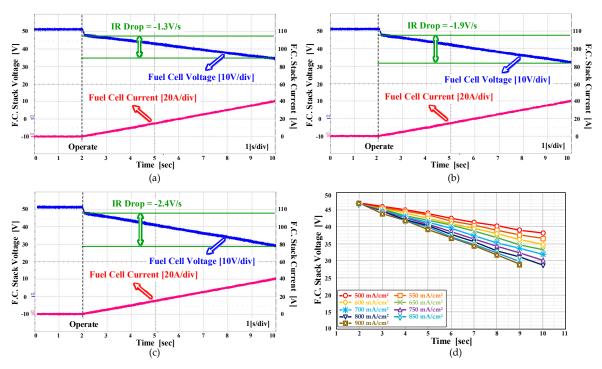

Figure 13. Fuel cell waveforms for current density of the (**a**) 500 mA/cm^2, (**b**) 700 mA/cm^2, (**c**) 900 mA/cm^2, and (**d**) voltage drop curve depending on current density of platinum catalyst.

Table 4. Characteristic experimental conditions of fuel cell.

Parameters	Values	Units
Hydrogen supply	70	[LPM]
Stack temperature	60	[°C]
Current density	500–900	[mA/cm^2]

4.3. The Experiment Results for Hybrid Fuel Cell Battery System and Forklift Drive

Based on the characteristics of each voltage drop, the experiment on the hydrogen recirculation of hybrid fuel cell battery system is performed. Figure 14 shows the hardware configuration of the hybrid fuel cell battery system for a forklift. It includes a battery management system (BMS) to monitor the battery's condition and the protection circuit module (PCM).
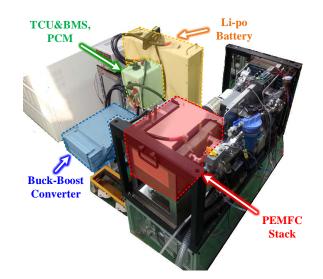

Figure 14. Experiment hardware configuration of hybrid fuel cell battery system.

Figure 15a shows fuel cell shutdown due to voltage drop when the voltage drop compensation method is not applied during hydrogen recirculation. When the fuel cell performs hydrogen recirculation, a rapid voltage drop to 28 V occurs. Then, shutdown of the fuel cell is occurred that stops all system operations.
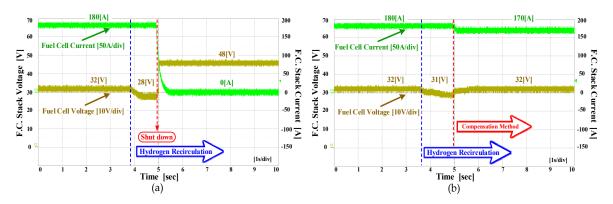

Figure 15. Output waveforms during hydrogen recirculation (**a**) not applied compensation method and (**b**) applied proposed compensation method.

Figure 15b shows the fuel cell output waveform when the proposed voltage drop compensation method is applied. When the voltage drop occurs, it can be confirmed that the voltage is restored

by reducing the current reference from 180 A to 170 A, thereby preventing shutdown of the fuel cell during hydrogen recirculation.

Figure 16 shows the output waveform of the lithium polymer battery. As the current of the fuel cell decreases, the lithium polymer battery supplies additional current, as shown in Figure 16. Therefore, constant power can be supplied to the load.
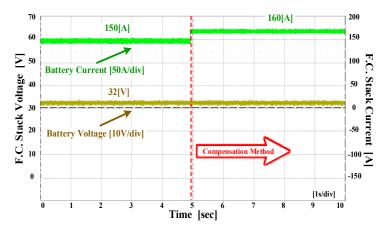

Figure 16. Output waveforms of lithium polymer battery during hydrogen recirculation.

Figure 17a shows the forklift with hybrid fuel cell battery system. The experimental method is lifting a 5 ton weight and driving at 25 km/h. The drive experiment of forklift was repeated six times.
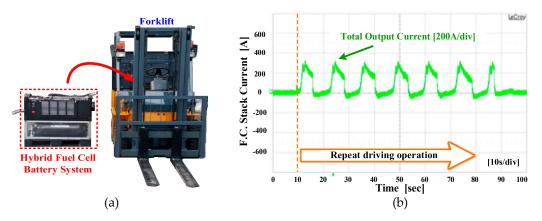

(a)　　　　　　　　　　　　　　　　　　　　(b)

Figure 17. (**a**) The forklift with hybrid fuel cell battery system and (**b**) the total output current of the hybrid fuel cell battery system during forklift operation.

Figure 17b shows the total output current of the hybrid fuel cell battery system flowing through the inverter, while the forklift operates; when lifting 5 tons and driving at 25 km/h, the forklift requires a current of 300 A or more maximally. However, it can be seen that the hybrid fuel cell battery system works normally without the shutdown during hydrogen recirculation, thanks to the proposed voltage drop compensation method.

5. Conclusions

In this paper, a fuel cell voltage drop compensation method is proposed. During hydrogen recirculation, voltage drop occurs due to various factors and causes shutdown of the fuel cell. To solve these problems, three factors to inducing voltage drop of fuel cell (the amount of hydrogen supply, the temperature of fuel cell stack, and the current density of platinum catalyst) were analyzed. Using the analyzed three factors, the voltage drop was calculated and compensated by controlling the output current of the buck-boost converter used in the fuel cell system. At this time, the current of the lithium

polymer battery increases as the current of the fuel cell decreases. Thereby, constant power is supplied to the load.

To verify the feasibility and effectiveness of the proposed voltage drop compensation method, the simulation was performed depicting the hybrid fuel cell battery system. Stable operation during hydrogen recirculation was verified by the fuel cell system and the drive experiments of the forklift. Conventional control method occurs voltage drop from 32 V to 28 V during hydrogen recirculation, which can cause fuel cell system breakdown. However, the shutdown problem was solved by using the proposed compensation method, and the operation stability of the fuel cell system depending on the various conditions was improved. Through this, the consumption of hydrogen fuel can be reduced by improving the stability of the fuel cell system, unlike in the past, when excessive hydrogen fuel was used. Given the experimental results, the proposed voltage drop compensation method could be a good candidate for commercial fuel cell systems.

Author Contributions: T.-H.E., M.-H.S. conceived and designed the experiment; T.-H.E., J.-W.K., J.-T.K. and J.-H.L. analyzed the theory; T.-H.E. wrote the manuscript; J.-T.K., C.-Y.W. participated in the research plan development and revised the manuscript. All authors have contributed to the manuscript.

Conflicts of Interest: The authors declare no conflict of interest.

References

1. Wang, S.; Guo, Y.; Dorrell, D. Analysis of rectangular EV inductive charging coupler. In Proceedings of the 2017 12th IEEE Conference on Industrial Electronics and Applications (ICIEA), Siem Reap, Cambodia, 18–20 June 2017; pp. 285–291.
2. Zheng, J.; Wang, X.; Men, K.; Zhu, C.; Zhu, S. Aggregation Model-Based Optimization for Electric Vehicle Charging Strategy. *IEEE Trans. Smart Grid* **2013**, *4*, 1058–1066. [CrossRef]
3. Abdulaal, A.; Cintuglu, M.H.; Asfour, S.; Mohammed, O.A. Solving the Multivariant EV Routing Problem Incorporating V2G and G2V Options. *IEEE Trans. Transp. Electrif.* **2017**, *3*, 238–248. [CrossRef]
4. Repp, S.; Harputlu, E.; Gurgen, S.; Castellano, M.; Kremer, N.; Pompe, N.; Wörner, J.; Hoffmann, A.; Thomann, R.; Emen, F.M. Synergetic effects of Fe_{3+} doped spinel $Li_4Ti_5O_{12}$ nanoparticles on reduced graphene oxide for high surface electrode hybrid supercapacitors. *Nanoscale* **2018**, *10*, 1877–1884. [CrossRef] [PubMed]
5. Genc, R.; Alas, M.O.; Harputlu, E.; Repp, S.; Kremer, N.; Castellano, M.; Colak, S.G.; Ocakoglu, K.; Erdem, E. High-capacitance hybrid supercapacitor based on multi-colored fluorescent carbon-dots. *Sci. Rep.* **2017**, *7*, 11222. [CrossRef] [PubMed]
6. Huffstutler, J.; Wasala, M.; Richie, J.; Barron, J.; Winchester, A.; Ghosh, S.; Yang, C.; Xu, W.; Song, L.; Kar, S.; et al. High Performance Graphene-Based Electrochemical Double Layer Capacitors Using 1-Butyl-1-methylpyrrolidinium tris (pentafluoroethyl) trifluorophosphate Ionic Liquid as an Electrolyte. *Electronics* **2018**, *7*, 229. [CrossRef]
7. Kamal, T.; Karabacak, M.; Hassan, S.; Fernández-Ramírez, L.; Riaz, M.; Khan, M.; Khan, L. Energy Management and Switching Control of PHEV Charging Stations in a Hybrid Smart Micro-Grid System. *Electronics* **2018**, *7*, 156. [CrossRef]
8. Kuehne, P.; Wenske, M.; Heuer, M.; Wolter, M. Unitized reversible PEM fuel cells for flexible electrical energy storage. In Proceedings of the International ETG Congress 2017, Bonn, Germany, 28–29 November 2017; pp. 1–6.
9. Lai, J.S.; Ellis, M.W. Fuel Cell Power Systems and Applications. *Proc. IEEE* **2017**, *105*, 2166–2190. [CrossRef]
10. Zhang, Z.; Mortensen, H.H.; Jensen, J.V.; Andersen, M.A.E. Fuel Cell and Battery Powered Forklifts. In Proceedings of the 2013 IEEE Vehicle Power and Propulsion Conference (VPPC), Beijing, China, 15–18 October 2013; pp. 1–5.

11. Shin, M.H.; Eom, T.H.; Park, Y.H.; Won, C.Y. Design and control of fuel cell-battery hybrid system for forklift. In Proceedings of the 2016 IEEE Transportation Electrification Conference and Expo, Asia-Pacific (ITEC Asia-Pacific), Busan, Korea, 1–4 June 2016; pp. 584–589.

12. Graber, G.; Galdi, V.; Calderaro, V.; Piccolo, A. A method to size the stack and the battery of a fuel cell vehicle reducing the fuel consumption. In Proceedings of the 2017 AEIT International Annual Conference, Cagliari, Italy, 20–22 September 2017; pp. 1–6.

13. Lewis, M.; Hearn, C.; Feng, X.; Hanlin, J.; Levin, J.; Ambrosio, J.; Guggenheim, P.; Walker, C. Design and modeling for hydrogen fuel cell conversion of parcel delivery trucks. In Proceedings of the 2017 IEEE Transportation Electrification Conference and Expo (ITEC), Chicago, IL, USA, 26–28 June 2017; pp. 674–678.

14. D'Ovidio, G.; Masciovecchio, C.; Rotondale, A. Hydrogen fuel cell and kinetic energy recover systems technologies for powering urban bus with zero emission energy cycle. *IET Intell. Transp. Syst.* **2016**, *10*, 573–578. [CrossRef]

15. Vasallo, M.J.; Andujar, J.M.; Garcia, C.; Brey, J.J. A Methodology for Sizing Backup Fuel-Cell/Battery Hybrid Power Systems. *IEEE Trans. Ind. Electron.* **2010**, *57*, 1964–1975. [CrossRef]

16. Khaligh, A.; Rahimi, A.M.; Lee, Y.J.; Cao, J.; Emadi, A.; Andrews, S.D.; Robinson, C.; Finnerty, C. Digital Control of an Isolated Active Hybrid Fuel Cell/Li-Ion Battery Power Supply. *IEEE Trans. Veh. Technol.* **2007**, *56*, 3709–3721. [CrossRef]

17. Zaidi, S.J. Research trends in polymer electrolyte membranes for PEMFC. In *Polymer Membranes for Fuel Cells*; Springer: Boston, MA, USA, 2009; pp. 7–25.

18. Owejan, J.P.; Gagliardo, J.J.; Sergi, J.M.; Kandlikar, S.G.; Trabold, T.A. Water management studies in PEM fuel cells, Part I: Fuel cell design and in situ water distributions. *Int. J. Hydrogen Energy* **2009**, *34*, 3436–3444. [CrossRef]

19. Pandiyan, S.; Jayakumar, K.; Rajalakshmi, N.; Dhathathreyan, K.S. Thermal and electrical energy management in a PEMFC stack–An analytical approach. *Int. J. Heat Mass Transf.* **2008**, *51*, 469–473. [CrossRef]

20. Hussain, M.M.; Baschuk, J.J.; Li, X.; Dincer, I. Thermodynamic analysis of a PEM fuel cell power system. *Int. J. Therm. Sci.* **2005**, *44*, 903–911. [CrossRef]

21. Lee, Y.; Kim, B.; Kim, Y. An experimental study on water transport through the membrane of a PEFC operating in the dead-end mode. *Int. J. Hydrogen Energy* **2009**, *34*, 7768–7779. [CrossRef]

22. Chen, J.; Siegel, J.B.; Stefanopoulou, A.G.; Waldecker, J.R. Optimization of purge cycle for dead-ended anode fuel cell operation. *Int. J. Hydrogen Energy* **2013**, *38*, 5092–5105. [CrossRef]

23. Spernjak, D.; Prasad, A.K.; Advani, S.G. Experimental investigation of liquid water formation and transport in a transparent single-serpentine PEM fuel cell. *J. Power Sources* **2007**, *170*, 334–344. [CrossRef]

24. Bradley, T.H.; Moffitt, B.A.; Mavris, D.N.; Parekh, D.E. Development and experimental characterization of a fuel cell powered aircraft. *J. Power Sources* **2007**, *171*, 793–801. [CrossRef]

25. Siegel, J.B.; McKay, D.A.; Stefanopoulou, A.G.; Hussey, D.S.; Jacobson, D.L. Measurement of liquid water accumulation in a PEMFC with dead-ended anode. *J. Electrochem. Soc.* **2008**, *155*, B1168–B1178. [CrossRef]

26. Matsuura, T.; Chen, J.; Siegel, J.B.; Stefanopoulou, A.G. Degradation phenomena in PEM fuel cell with dead-ended anode. *Int. J. Hydrogen Energy* **2013**, *38*, 11346–11356. [CrossRef]

27. Han, I.; Jeong, J.; Shin, H.K. PEM fuel-cell stack design for improved fuel utilization. *Int. J. Hydrogen Energy* **2013**, *38*, 11996–12006. [CrossRef]

28. Wei, Y.C.; Chen, Y. A mathematical model to study the performance of a proton exchange membrane fuel cell in a dead-ended anode mode. *Appl. Energy* **2014**, *130*, 113–121.

29. Siegel, J.B. Experiments and Modeling of PEM Fuel Cells for Dead-Ended Anode Operation. Ph.D. Thesis, University of Michigan, Ann Arbor, MI, USA, 2010.

30. Tüber, K.; Pócza, D.; Hebling, C. Visualization of water buildup in the cathode of a transparent PEM fuel cell. *J. Power Sources* **2003**, *124*, 403–414. [CrossRef]

31. Gomez, A.; Raj, A.; Sasmito, A.P.; Shamim, T. Effect of operating parameters on the transient performance of a polymer electrolyte membrane fuel cell stack with a dead-end anode. *Appl. Energy* **2014**, *130*, 692–701. [CrossRef]

32. Ebadighajari, A.; Homayouni, H.; DeVaal, J.; Golnaraghi, F. Model Predictive Control of Polymer Electrolyte Membrane fuel cell with dead-end anode and periodic purging. In Proceedings of the 2016 IEEE Conference on Control Applications (CCA), Nice, France, 8–10 October 2016.

33. Chen, J.; Siegel, J.B.; Stefanopoulou, A.G. Nitrogen blanketing front equilibria in dead end anode fuel cell operation. In Proceedings of the American Control Conference (ACC), San Francisco, CA, USA, 29 June–1 July 2011.

34. Himanen, O.; Hottinen, T.; Tuurala, S. Operation of a planar free-breathing PEMFC in a dead-end mode. *Electrochem. Commun.* **2007**, *9*, 891–894. [CrossRef]

35. Hearn, C.S.; Lewis, M.C.; Thompson, R.T.; Chen, D.; Hanlm, J.; Zuckerman, D.; Lindsay, T. Design and demonstration of an extended range hydrogen fuel cell utility vehicle. In Proceedings of the 2011 IEEE Vehicle Power and Propulsion Conference, Chicago, IL, USA, 6–9 September 2011; pp. 1–5.

36. Dallago, E.; Danioni, A.; Passoni, M.; Venchi, G. Comparison of transient performance in a peak current-mode flyback converter. In Proceedings of the 2002 IEEE International Symposium on Industrial Electronics, ISIE 2002, L'Aquila, Italy, 8–11 July 2002; Volume 4, pp. 1049–1052.

37. Chen, T.H.; Lin, W.L.; Liaw, C.M. Dynamic modeling and controller design of flyback converter. *IEEE Trans. Aerosp. Electron. Syst.* **1999**, *35*, 1230–1239. [CrossRef]

38. Kleebchampee, W.; Bunlaksananusorn, C. Modeling and Control Design of a Current-Mode Controlled Flyback Converter with Optocoupler Feedback. In Proceedings of the 2005 International Conference on Power Electronics and Drives Systems, Kuala Lumpur, Malaysia, 28 November–1 December 2005; pp. 787–792.

39. Shen, C.L.; Chiu, P.C. Buck-boost-flyback integrated converter with single switch to achieve high voltage gain for PV or fuel-cell applications. *IET Power Electron.* **2016**, *9*, 1228–1237. [CrossRef]

40. Ebadighajari, A.; DeVaal, J.; Golnaraghi, F. Reduction of hydrogen transfer by constrained control of anode hydrogen recirculation in a polymer electrolyte membrane fuel cell. In Proceedings of the 2017 IEEE 56th Annual Conference on Decision and Control (CDC), Melbourne, VIC, Australia, 12–15 December 2017; pp. 1440–1445.

41. Ross, D.K. Hydrogen storage: The major technological barrier to the development of hydrogen fuel cell cars. *Vacuum* **2006**, *80*, 1084–1089. [CrossRef]

42. Li, X.; Xiao, M.; Choe, S.-Y. Reduced order of electrochemical model for a pouch type high power Li-polymer battery. In Proceedings of the 2011 International Conference on Clean Electrical Power (ICCEP), Ischia, Italy, 14–16 June 2011.

43. Zhang, S.; Yuan, X.Z.; Hin, J.N.; Wang, H.; Friedrich, K.A.; Schulze, M. A review of platinum-based catalyst layer degradation in proton exchange membrane fuel cells. *J. Power Sources* **2009**, *194*, 588–600. [CrossRef]

44. Shao, Y.; Yin, G.; Gao, Y. Understanding and approaches for the durability issues of Pt-based catalysts for PEM fuel cell. *J. Power Sources* **2007**, *171*, 558–566. [CrossRef]

45. Cho, Y.H.; Park, H.S.; Cho, Y.H.; Jung, D.S.; Park, H.Y.; Sung, Y.E. Effect of platinum amount in carbon supported platinum catalyst on performance of polymer electrolyte membrane fuel cell. *J. Power Sources* **2007**, *172*, 89–93. [CrossRef]